

1 **Quantifying the nitrogen isotope effects during photochemical**
2 **equilibrium between NO and NO₂: implications for δ¹⁵N in**
3 **tropospheric reactive nitrogen**

4 Jianghanyang Li¹, Xuan Zhang², John Orlando², Geoffrey Tyndall² and Greg Michalski^{1,3}

5 ¹ Department of Earth, Atmospheric and Planetary Sciences, Purdue University, West Lafayette,
6 IN, 47907

7 ² Atmospheric Chemistry Observations and Modeling Lab, National Center for Atmospheric
8 Research, Boulder, CO, 80301

9 ³ Department of Chemistry, Purdue University, West Lafayette, IN, 47907

10 *Correspondence to:* Jianghanyang Li (li2502@purdue.edu)

11 **Abstract.** Nitrogen isotope fractionations between nitrogen oxides (NO and NO₂) play a
12 significant role in determining the nitrogen isotopic compositions (δ¹⁵N) of atmospheric reactive
13 nitrogen. Both the equilibrium isotopic exchange between NO and NO₂ molecules and the isotope
14 effects occurring during the NO_x photochemical cycle are important, but both are not well
15 constrained. The nighttime and daytime isotopic fractionations between NO and NO₂ in an
16 atmospheric simulation chamber at atmospherically relevant NO_x levels were measured. Then, the
17 impact of NO_x level and NO₂ photolysis rate to the combined isotopic fractionation (equilibrium
18 isotopic exchange and photochemical cycle) between NO and NO₂ were calculated. It was found
19 that the isotope effects occurring during the NO_x photochemical cycle can be described using a
20 single fractionation factor, designated the Leighton Cycle Isotope Effect (LCIE). The results
21 showed that at room temperature, the fractionation factor of nitrogen isotopic exchange is
22 1.0275±0.0012, and the fractionation factor of LCIE (when O₃ solely controls the oxidation from
23 NO to NO₂) is 0.990±0.005. The measured LCIE factor showed good agreement with previous
24 field measurements, suggesting that it could be applied in ambient environment, although future
25 work is needed to assess the isotopic fractionation factors of NO + RO₂/HO₂ → NO₂. The results
26 were used to model the NO-NO₂ isotopic fractionations under several NO_x conditions. The model
27 suggested that isotopic exchange was the dominate factor when NO_x >20 nmol mol⁻¹, while LCIE
28 was more important at low NO_x concentrations (<1 nmol mol⁻¹) and high rates of NO₂ photolysis.
29 These findings provided a useful tool to quantify the isotopic fractionations between tropospheric
30 NO and NO₂, which can be applied in future field observations and atmospheric chemistry models.

31

32

33 1. Introduction

34 The nitrogen isotopic composition ($\delta^{15}\text{N}$) of reactive nitrogen compounds in the
35 atmosphere is an important tool in understanding the sources and chemistry of atmospheric NO_x
36 ($\text{NO}+\text{NO}_2$). It has been suggested that the $\delta^{15}\text{N}$ value of atmospheric nitrate (HNO_3 , nitrate
37 aerosols and nitrate ions in the precipitation and snow) imprints the $\delta^{15}\text{N}$ value of NO_x sources
38 (Elliott et al., 2009; Kendall et al., 2007) thus many studies have used the $\delta^{15}\text{N}$ values of
39 atmospheric nitrate to investigate NO_x sources (Chang et al., 2018; Felix et al., 2012; Felix &
40 Elliott, 2014; Gobel et al., 2013; Hastings et al., 2004, 2009; Morin et al., 2009; Park et al., 2018;
41 Walters et al., 2015, 2018). However, there remain questions about how isotopic fractionations
42 that may occur during photochemical cycling of NO_x could alter the $\delta^{15}\text{N}$ values as it partitions
43 into NO_y (NO_y = atmospheric nitrate, NO_3 , N_2O_5 , HONO , etc., Chang et al., 2018; Freyer, 1991;
44 Hastings et al., 2004; Jarvis et al., 2008; Michalski et al., 2005; Morin et al., 2009; Zong et al.,
45 2017). Similarly, other complex reactive nitrogen chemistry, such as nitrate photolysis and re-
46 deposition in ice and snow (Frey et al., 2009), may impact the $\delta^{15}\text{N}$ of NO_y and atmospheric nitrate.
47 The fractionation between NO and NO_2 via isotope exchange has been suggested to be the
48 dominant factor in determining the $\delta^{15}\text{N}$ of NO_2 and ultimately atmospheric nitrate (Freyer, 1991;
49 Freyer et al., 1993; Savarino et al., 2013; Walters et al., 2016). However, isotopic fractionations
50 occur in most, if not all, NO_x and NO_y reactions, while most of these are still unknown or, if
51 calculated (Walters and Michalski, 2015), unverified by experiments. Since the atmospheric
52 chemistry of NO_y varies significantly in different environments (e.g., polluted vs. pristine, night
53 vs. day), the isotopic fractionations associated with NO_y chemistry are also likely to vary in
54 different environments. These unknowns could potentially bias conclusions about NO_x source
55 apportionment reached when using nitrogen isotopes. Therefore, understanding the isotopic

56 fractionations between NO and NO₂ during photochemical cycling could improve our
57 understanding of the relative role of sources versus chemistry for controlling the δ¹⁵N variations
58 of atmospheric NO₂ and nitrate.

59 In general, there are three types of isotopic fractionation effects associated with NO_x
60 chemistry (Fig. 1A). The first type is the equilibrium isotopic effect (EIE), i.e., isotope exchange
61 between two compounds without forming new molecules (Urey, 1947, Bigeleisen and Mayer,
62 1947), which for nitrogen isotopes in the NO_x system is the $^{15}\text{NO} + ^{14}\text{NO}_2 \leftrightarrow ^{14}\text{NO} + ^{15}\text{NO}_2$
63 exchange reaction (Begun and Melton, 1956, Walters et al., 2016). The second type is the kinetic
64 isotopic effect (KIE) associated with difference in isotopologue rate coefficients during
65 unidirectional reactions (Bigeleisen & Wolfsberg, 1957). In the NO_x system this KIE would
66 manifest in the oxidation of NO into NO₂ by O₃/HO₂/RO₂. The third type is the photochemical
67 isotope fractionation effect (PHIFE, Miller & Yung, 2000), which for NO_x is the isotopic
68 fractionation associated with NO₂ photolysis. All three fractionations could impact the δ¹⁵N value
69 of NO₂, and consequently atmospheric nitrate, but the relative importance of each may vary.

70 The limited number of studies on the EIE in the NO_x cycle have significant uncertainties.
71 Discrepancies in the EIE for $^{15}\text{NO} + ^{14}\text{NO}_2 \leftrightarrow ^{14}\text{NO} + ^{15}\text{NO}_2$ have been noted in several studies.
72 Theoretical calculations predicted isotope fractionation factors (α) ranging from 1.035 to 1.042 at
73 room temperature (Begun & Fletcher, 1960; Monse et al., 1969; Walters & Michalski, 2015) due
74 to the different approximations used to calculate harmonic frequencies in each study. Likewise,
75 two separate experiments measured different room temperature fractionation factors of
76 1.028 ± 0.002 (Begun & Melton, 1956) and 1.0356 ± 0.0015 (Walters et al., 2016). A concern in both
77 experiments is that they were conducted in small chambers with high NO_x concentrations
78 (hundreds of μmol mol⁻¹), significantly higher than typical ambient atmospheric NO_x levels

79 (usually less than $0.1 \mu\text{mol mol}^{-1}$). Whether the isotopic fractionation factors determined by these
80 experiments are applicable in the ambient environment is uncertain because of possible wall effects
81 and formation of higher oxides, notably N_2O_4 and N_2O_3 at these high NO_x concentrations.

82 Even less research has examined the KIE and PHIFE occurring during NO_x cycling. The
83 KIE of $\text{NO} + \text{O}_3$ has been theoretically calculated (Walters and Michalski, 2016) but has not been
84 experimentally verified. The NO_2 PHIFE has not been experimentally determined or theoretically
85 calculated. As a result, field observation studies often overlook the effects of PHIFE and KIE.
86 Freyer et al. (1993) measured NO_x concentrations and the $\delta^{15}\text{N}$ values of NO_2 over a 1-year period
87 at Jülich, Germany and inferred a combined NO_x isotope fractionation factor (EIE+KIE+PHIFE)
88 of 1.018 ± 0.001 . Freyer et al. (1993) suggested that the NO_x photochemical cycle (KIE and PHIFE)
89 tends to diminish the equilibrium isotopic fractionation (EIE) between NO and NO_2 . Even if this
90 approach were valid, applying this single fractionation factor elsewhere, where NO_x , O_3
91 concentrations and actinic fluxes are different, would be tenuous given that these factors may
92 influence the relative importance of EIE, KIE and PHIFE (Hastings et al., 2004; Walters et al.,
93 2016). Therefore, to quantify the overall isotopic fractionations between NO and NO_2 at various
94 tropospheric conditions, it is crucial to know 1) isotopic fractionation factors of EIE, KIE and
95 PHIFE individually and 2) the relative importance of each factor under various conditions.

96 In this work, we aim to quantify the nitrogen isotope fractionation factors between NO and
97 NO_2 at photochemical equilibrium. First, we measure the N isotope fractionations between NO
98 and NO_2 in an atmospheric simulation chamber at atmospherically relevant NO_x levels. Then, we
99 provide mathematical solutions to assess the impact of NO_x level and NO_2 photolysis rate ($j(\text{NO}_2)$)
100 to the relative importance of EIE, KIE and PHIFE. Subsequently we use the solutions and chamber
101 measurements to calculate the isotopic fractionation factors of EIE, KIE and PHIFE. Lastly, using

102 the calculated fractionation factors and the equations, we model the NO-NO₂ isotopic
103 fractionations at several sites to illustrate the behavior of $\delta^{15}\text{N}$ values of NO_x in the ambient
104 environment.

105

106 **2. Methods**

107 The experiments were conducted using a 10 m³ Atmospheric Simulation Chamber at the
108 National Center for Atmospheric Research (see descriptions in supplementary material and Zhang
109 et al. (2018)). A set of mass flow controllers was used to inject NO and O₃ into the chamber. NO
110 was injected at 1 L min⁻¹ from an in-house NO/N₂ cylinder (133.16 $\mu\text{mol mol}^{-1}$ NO in ultra-pure
111 N₂), and O₃ was generated by flowing 5 L min⁻¹ zero-air through a flow tube equipped with a UV
112 Pen-Ray lamp (UVP LLC., CA) into the chamber. NO and NO₂ concentrations were monitored in
113 real time by chemiluminescence with a detection limit of 0.5 ppb (model CLD 88Y, Eco Physics,
114 MI) as were O₃ concentrations using an UV absorption spectroscopy with a detection limit of 0.5
115 ppb (model 49, Thermo Scientific, CO). In each experiment, the actual amounts of NO and O₃
116 injected were calculated using measured NO_x and O₃ concentrations after steady state was reached
117 (usually within 1 h). The wall loss rate of NO₂ was tested by monitoring O₃ (29 nmol mol⁻¹) and
118 NO_x (62 nmol mol⁻¹) over a 4-hour period. After the NO and NO₂ concentrations reached steady
119 state, no decrease in NO₂ concentrations was observed showing that chamber wall loss was
120 negligible.

121 Two sets of experiments were conducted to separately investigate the EIE, KIE and PHIFE.
122 The first set of experiments was conducted in the dark. In each of these dark experiments, a range
123 of NO and O₃ ($[\text{O}_3] < [\text{NO}]$) was injected into the chamber to produce NO-NO₂ mixtures with
124 $[\text{NO}]/[\text{NO}_2]$ ratios ranging from 0.43 to 1.17. The N isotopes of these mixtures were used to

125 investigate the EIE between NO and NO₂. The second set of experiments was conducted under
126 irradiation of UV lights (300-500 nm, see supplementary material for irradiation spectrum). Under
127 such conditions, NO, NO₂ and O₃ reached photochemical steady state, which combined the
128 isotopic effects of EIE, KIE and PHIFE. In addition, three experiments were conducted to measure
129 the $\delta^{15}\text{N}$ value of the tank NO. In each of these experiments, a certain amount of O₃ was first
130 injected into the chamber, then approximately the same amount of NO was injected into the
131 chamber to ensure 100% of the NO_x was in the form of NO₂ with little O₃ (<3 nmol mol⁻¹)
132 remaining in the chamber, such that the O₃+NO₂ reaction was negligible. The NO₂ in the chamber
133 was then collected and its $\delta^{15}\text{N}$ value measured, which equates to the $\delta^{15}\text{N}$ value of the tank NO.

134 In all experiments, the concentrations of NO, NO₂ and O₃ were allowed to reach steady
135 state, and the product NO₂ was collected from the chamber using a honeycomb denuder tube. The
136 glass denuder tubes (Chemcomb 3500, Thermo Fisher Scientific) were coated with a solution of
137 10% KOH and 25% guaiacol in methanol and then dried by flowing N₂ gas through the denuder
138 tube for 15 seconds (Williams and Grosjean, 1990, Walters et al., 2016). The NO₂ reacted with
139 guaiacol coating and was converted into NO₂⁻ that was retained on the denuder tube wall (Williams
140 and Grosjean, 1990). NO was inert to the denuder tube coating: a control experiment sampled pure
141 NO using the denuder tubes, which did not show any measurable NO₂⁻. The NO₂ collection
142 efficiency of a single honeycomb denuder tube was tested in another control experiment: air
143 containing 66 nmol mol⁻¹ of NO₂ was drawn out of the chamber through a denuder tube, and the
144 NO₂ concentration at the exit of the tube holder was measured and found to be below the detection
145 limit (<1 nmol mol⁻¹), suggesting the collection efficiency was nearly 100% when [NO₂] <66 nmol
146 mol⁻¹. Furthermore, when the denuder system consisted of two denuder tubes in series and NO₂⁻ in
147 the second denuder was below the detection limit indicating trivial NO₂ breakthrough. The NO₂⁻

148 was leached from each denuder tube by rinsing thoroughly with 10 ml deionized water into a clean
149 polypropylene container and stored frozen until isotopic analysis. Isotopic analysis was conducted
150 at Purdue Stable Isotope Laboratory. For each sample, approximately 50 nmol of the NO_2^- extract
151 was mixed with 2 M sodium azide solution in acetic acid buffer in an air-tight glass vial, then
152 shaken overnight to completely reduce all the NO_2^- to $\text{N}_2\text{O}_{(g)}$ (Casciotti & McIlvin, 2007; McIlvin
153 & Altabet, 2005). The product N_2O was directed into a Thermo GasBench equipped with cryo-
154 trap, then the $\delta^{15}\text{N}$ of the N_2O was measured using a Delta-V Isotope Ratios Mass Spectrometer.
155 Six coated denuders tubes that did not get exposed to NO_2 were also analyzed using the same
156 chemical procedure, which did not show any measurable signal on the IRMS, suggesting the blank
157 from both sampling process and the chemical conversion process was negligible. The overall
158 analytical uncertainty for $\delta^{15}\text{N}$ analysis was $\pm 0.5 \text{ ‰}$ (1σ) based on replicate analysis of in house
159 NO_2^- standards.

160

161 3. Results and Discussions

162 3.1. Equilibrium Isotopic Fractionation between NO and NO_2

163 The equilibrium isotope fractionation factor, $\alpha(\text{NO}_2\text{-NO})$, is the ^{15}N enrichment in NO_2
164 relative to NO , and is expressed as the ratio of rate constants k_2 / k_1 of two reactions:



167 where k_1 is the rate constant of the isotopic exchange, which was previously determined to be
168 $8.14 \times 10^{-14} \text{ cm}^3 \text{ s}^{-1}$ (Sharma et al., 1970). The reaction time required for NO-NO_2 to reach isotopic
169 equilibrium was estimated using the exchange rate constants in a simple kinetics box model
170 (BOXMOX, Knote et al., 2015). The model predicts that at typical NO_x concentrations used during

171 the chamber experiments (7.7-62.4 nmol mol⁻¹), isotopic equilibrium would be reached within 15
 172 minutes (see supplementary material). Since the sample collection usually started 1 hour after NO_x
 173 was well mixed in the chamber, there was sufficient time to reach full isotope equilibrium. The
 174 isotope equilibrium fractionation factor is then calculated to be:

$$175 \quad \alpha(\text{NO}_2 - \text{NO}) = \frac{[^{15}\text{NO}_2] \times [^{14}\text{NO}]}{[^{14}\text{NO}_2] \times [^{15}\text{NO}]} = \frac{R(\text{NO}_2)}{R(\text{NO})} \quad \text{Eq. (1)}$$

176 where R(NO, NO₂) are the ¹⁵N/¹⁴N ratios of NO and NO₂. By definition, the
 177 δ¹⁵N(NO)=(R(NO)/R(reference) -1)×1000‰ and δ¹⁵N(NO₂)=(R(NO₂)/R(reference)-1) ×1000 ‰,
 178 but hereafter, the δ¹⁵N values of NO, NO₂ and NO_x will be referred as δ(NO), δ(NO₂) and δ(NO_x),
 179 respectively. Eq. (1) leads to:

$$180 \quad \delta(\text{NO}_2) - \delta(\text{NO}) = (\alpha(\text{NO}_2 - \text{NO}) - 1) \times 1000 \text{ ‰} \times (1 + \delta(\text{NO}))$$

$$181 \quad = \varepsilon(\text{NO}_2 - \text{NO}) \times (1 + \delta(\text{NO})) \quad \text{Eq. (2)}$$

182 where ε(NO₂-NO) is the isotope enrichment factor (ε(NO₂-NO) = (α(NO₂-NO)-1)×1000‰, Hoefs,
 183 2009). Using Eq. (2) and applying NO_x isotopic mass balance (δ(NO_x)=f(NO₂)×δ(NO₂)+(1-
 184 f(NO₂))×δ(NO)), f(NO₂)=[NO₂]/([NO]+[NO₂])) yields:

$$185 \quad \delta(\text{NO}_2) - \delta(\text{NO}_x) = \varepsilon(\text{NO}_2 - \text{NO}) \times (1 + \varepsilon(\text{NO}_2 - \text{NO})) \times (1 + \delta(\text{NO}_2)) \times (1 - f(\text{NO}_2)) \quad \text{Eq. (3)}$$

186 Here, δ(NO_x) equals to the δ¹⁵N value of the cylinder NO and f(NO₂) is the molar fraction of NO₂
 187 with respect to total NO_x. Three experiments (see descriptions in method section) that measured
 188 δ(NO_x) showed consistent δ(NO_x) values of -58.7±0.8 ‰ (n = 3), indicating δ(NO_x) remained
 189 unchanged throughout the experiments (as expected for isotope mass balance). Thus, the δ(NO_x)
 190 can be treated as a constant in Eq. (3), and the linear regression of (δ(NO₂)-δ(NO_x))/(1+δ(NO₂))
 191 versus 1-f(NO₂) should have an intercept of 0 and a slope of ε(NO₂-NO)/(1+ε(NO₂-NO)).

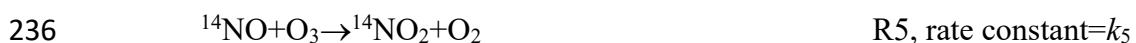
192 The plot of $(\delta(\text{NO}_2)-\delta(\text{NO}_x))/(1+\delta(\text{NO}_2))$ as a function of $1-f(\text{NO}_2)$ values from five
193 experiments yields an $\epsilon(\text{NO}_2\text{-NO})$ value of 27.5 ± 1.2 ‰ at room temperature (Fig. 1B). This
194 fractionation factor is comparable to previously measured values but with some differences. Our
195 result agrees well with the $\alpha(\text{NO}_2\text{-NO})$ value of 1.028 ± 0.002 obtained by Begun and Melton (1956)
196 at room temperature. However, Walters et al., (2016) determined the $\alpha(\text{NO}_2\text{-NO})$ values of NO-
197 NO_2 exchange in a 1-liter reaction vessel, which showed a slightly higher $\alpha(\text{NO}_2\text{-NO})$ value of
198 1.035. This discrepancy might originate from rapid heterogeneous reactions on the wall of the
199 reaction vessel at high NO_x concentrations and the small chamber size used by Walters et al. (2016).
200 They used a reaction vessel made of Pyrex, which is known to absorb water (Do Remus et al.,
201 1983; Takei et al., 1997) that can react with NO_2 forming HONO, HNO_3 and other N compounds.
202 Additionally, previous studies have suggested that Pyrex walls enhance the formation rate of N_2O_4
203 by over an order of magnitude (Barney & Finlayson-Pitts, 2000; Saliba et al., 2001), which at
204 isotopic equilibrium is enriched in ^{15}N compared to NO and NO_2 (Walters & Michalski, 2015).
205 Therefore, their measured $\alpha(\text{NO}_2\text{-NO})$ might be slightly higher than the actual $\alpha(\text{NO}_2\text{-NO})$ value.
206 In this work, the 10 m^3 chamber has a much smaller surface to volume ratio relative to Walters et
207 al. (2016) which minimizes wall effects, and the walls were made of Teflon that minimize NO_2
208 surface reactivity, which was evidenced by the NO_2 wall loss control experiment. Furthermore,
209 the low NO_x mixing ratios in our experiments minimized N_2O_4 and N_2O_3 formation. At NO and
210 NO_2 concentrations of 50 nmol mol^{-1} the steady state concentrations of N_2O_4 and N_2O_3 were
211 calculated to be 0.014 and $0.001\text{ pmol mol}^{-1}$, respectively (Atkinson et al., 2004). Therefore, we
212 suggest our measured $\alpha(\text{NO}_2\text{-NO})$ value (1.0275 ± 0.0012) may better reflect the room temperature
213 (298 K) NO- NO_2 EIE in the ambient environment.

214 Unfortunately, the chamber temperature could not be controlled so we were not able to
 215 investigate the temperature dependence of the EIE. Hence, we speculate that the $\alpha(\text{NO}_2\text{-NO})$
 216 follows a similar temperature dependence pattern calculated in Walters et al. (2016). Walters et al.
 217 (2016) suggested that, the $\varepsilon(\text{NO}_2\text{-NO})$ value would be 4.7 ‰ higher at 273 K and 2.0 ‰ lower at
 218 310 K, relative to room temperature (298 K). Using this pattern and our experimentally determined
 219 data, we suggest the $\alpha(\text{NO}_2\text{-NO})$ values at 273 K, 298 K and 310 K are 32.2 ± 1.2 ‰, 27.5 ± 1.2 ‰
 220 and 25.5 ± 1.2 ‰, respectively. This 6.7‰ variation at least partially contribute to the daily and
 221 seasonal variations of $\delta^{15}\text{N}$ values of NO_2 and nitrate in some areas (e.g., polar regions with strong
 222 seasonal temperature variation). Thus, future investigations should be conducted to verify the EIE
 223 temperature dependence.

224

225 3.2. Kinetic isotopic fractionation of Leighton Cycle

226 The photochemical reactions of NO_x will compete with the isotope exchange fractionations
 227 between NO and NO_2 . The NO-NO_2 photochemical cycle in the chamber was controlled by the
 228 Leighton cycle: NO_2 photolysis and the $\text{NO} + \text{O}_3$ reaction. This is because there were no VOCs in
 229 the chamber so no RO_2 was produced, which excludes the $\text{NO} + \text{RO}_2$ reaction. Likewise, the low
 230 water vapor content ($\text{RH} < 10\%$) and the minor flux of photons < 310 nm results in minimal OH
 231 production and hence little HO_2 formation and subsequently trivial amount of NO_2 would be
 232 formed by $\text{NO} + \text{HO}_2$. Applying these limiting assumptions, the EIE between NO and NO_2 (R1-
 233 R2) were only competing with the KIE (R3-R4) and the PHIFE in R5-R6:



237 $^{15}\text{NO} + \text{O}_3 \rightarrow ^{15}\text{NO}_2 + \text{O}_2$ R6, rate constant = $k_5 \times \alpha_2$

238 In which $j(\text{NO}_2)$ is the NO_2 photolysis rate ($1.4 \times 10^{-3} \text{ s}^{-1}$ in these experiments), k_5 is the rate constant
 239 for the $\text{NO} + \text{O}_3$ reaction ($1.73 \times 10^{-14} \text{ cm}^3 \text{ s}^{-1}$, Atkinson et al., 2004), and $\alpha_{1,2}$ are isotopic
 240 fractionation factors for the two reactions. Previous studies (Freyer et al., 1993; Walters et al.,
 241 2016) have attempted to assess the competition between EIE (R1-R2), KIE and PHIFE (R3-R6),
 242 but none of them quantified the relative importance of the two processes, nor were α_1 or α_2 values
 243 experimentally determined. Here we provide the mathematical solution of EIE, KIE and PHIFE to
 244 illustrate how R1-R6 affect the isotopic fractionations between NO and NO_2 .

245 First, the NO_2 lifetime with respect to isotopic exchange with NO (τ_{exchange}) and photolysis
 246 (τ_{photo}) was determined:

$$247 \quad \tau_{\text{exchange}} = \frac{1}{k_1 \times [\text{NO}]} \quad \text{Eq. (4)}$$

$$248 \quad \tau_{\text{photo}} = \frac{1}{j(\text{NO}_2)} \quad \text{Eq. (5)}$$

249 We then define an A factor:

$$250 \quad A = \begin{cases} \frac{\tau_{\text{exchange}}}{\tau_{\text{photo}}} & \text{when } j(\text{NO}_2) \neq 0 \\ 0 & \text{when } j(\text{NO}_2) = 0 \end{cases} \quad \text{Eq. (6)}$$

251 Using R1-R6 and Eq. (1)-(6), we solved steady-state $\delta(\text{NO}_2)$ and $\delta(\text{NO})$ values (see calculations
 252 in supplementary material). Our calculations show that the $\delta(\text{NO}_2) - \delta(\text{NO})$ and $\delta(\text{NO}_2) - \delta(\text{NO}_x)$
 253 values at steady state can be expressed as functions of α_1 , α_2 , $\alpha(\text{NO}_2 - \text{NO})$ and A:

$$254 \quad \delta(\text{NO}_2) - \delta(\text{NO}) (\text{‰}) = \frac{(\alpha_2 - \alpha_1) \times A + (\alpha(\text{NO}_2 - \text{NO}) - 1)}{A + 1} \times 1000 \text{ ‰} \quad \text{Eq. (7)}$$

$$255 \quad \delta(\text{NO}_2) - \delta(\text{NO}_x) (\text{‰}) = \frac{(\alpha_2 - \alpha_1) \times A + (\alpha(\text{NO}_2 - \text{NO}) - 1)}{A + 1} \times (1 - f(\text{NO}_2)) \times 1000 \text{ ‰} \quad \text{Eq. (8)}$$

256 Equation (7) shows the isotopic fractionation between NO and NO_2 ($\delta(\text{NO}_2) - \delta(\text{NO})$) is largely
 257 determined by A, the EIE factor ($\alpha(\text{NO}_2 - \text{NO}) - 1$) and the $(\alpha_2 - \alpha_1)$ factor. This $(\alpha_2 - \alpha_1)$ represents a

258 combination of KIE and PHIFE, suggesting they act together as one factor; therefore, we name the
259 (α_2 - α_1) factor Leighton Cycle Isotopic Effect, i.e., LCIE. Using measured $\delta(\text{NO}_2)$ - $\delta(\text{NO})$ values,
260 A values, and the previously determined EIE factor, we calculated that the best fit for the LCIE
261 factor was -10 ± 5 ‰ (showing the lowest Rooted Mean Square Error, RMSE, of 1.1‰, Fig. 1C).
262 The uncertainties in the LCIE factor are relatively higher than that of the EIE factor, mainly
263 because of the accumulated analytical uncertainties at low NO_x and O_3 concentrations, and low A
264 values (0.10-0.28) due to the relatively low $j(\text{NO}_2)$ value ($1.4 \times 10^{-3} \text{ s}^{-1}$) under the chamber
265 irradiation conditions.

266 This LCIE factor determined in our experiments is in good agreement with theoretical
267 calculations. Walters and Michalski (2016) previously used an *ab initio* approach to determine an
268 α_2 value of 0.9933 at room temperature, 0.9943 at 237 K and 0.9929 at 310 K. The variation of α_2
269 values from 273 K to 310 K is only ± 0.7 ‰, significantly smaller than our experimental uncertainty.
270 The α_1 value was calculated using a ZPE shift model (Miller & Yung, 2000) to calculate the
271 isotopic fractionation of NO_2 by photolysis. Briefly, this model assumes both isotopologues have
272 the same quantum yield function and the PHIFE was only caused by the differences in the $^{15}\text{NO}_2$
273 and $^{14}\text{NO}_2$ absorption cross-section as a function of wavelength, thus α_1 values do not vary by
274 temperature. The $^{15}\text{NO}_2$ absorption cross-section was calculated by shifting the $^{14}\text{NO}_2$ absorption
275 cross-section by the $^{15}\text{NO}_2$ zero-point energy (Michalski et al., 2004). When the ZPE shift model
276 was used with the irradiation spectrum of the chamber lights, the resulting α_1 value was 1.0023.
277 Therefore, the theoretically predicted α_2 - α_1 value should be -0.0090, i.e., -9.0 ± 0.7 ‰ when
278 temperature ranges from 273 K to 310 K. This result shows excellent agreement with our
279 experimentally determined room temperature α_2 - α_1 value of -10 ± 5 ‰.

280 This model was then used to evaluate the variations of α_1 value to different lighting
281 conditions. The TUV model (TUV5.3.2, Madronich & Flocke, 1999) was used to calculate the
282 solar wavelength spectrum at three different conditions: early morning/late afternoon (solar zenith
283 angle=85 degree), mid-morning/afternoon (solar zenith angle=45 degree), noon (solar zenith
284 angle=0 degree). These spectrums were used in the ZPE shift model to calculate the α_1 values,
285 which are 1.0025, 1.0028, and 1.0029 at solar zenith angles of 85, 45 and 0 degree, respectively.
286 These values, along with the predicted α_1 value in the chamber, showed a total span of 0.6‰
287 (1.0026 ± 0.0003), which is again significantly smaller than our measured uncertainty. Therefore,
288 we suggest that our experimentally determined LCIE factor (-10 ± 5 ‰) can be used in most
289 tropospheric solar irradiation spectrums.

290 The equations can also be applied in tropospheric environments to calculate the combined
291 isotopic fractionations of EIE and LCIE for NO and NO₂. First, the NO₂ sink reactions (mainly
292 NO₂+OH in the daytime) are at least 2-3 orders of magnitude slower than the Leighton cycle and
293 the NO-NO₂ isotope exchange reactions (Walters et al., 2016), therefore their effects on the $\delta(\text{NO}_2)$
294 should be minor. Second, although the conversion of NO into NO₂ in the ambient environment is
295 also controlled by NO + RO₂ and HO₂ in addition to NO+O₃ (e.g., King et al., 2001), Eq. (7) still
296 showed good agreement with field observations in previous studies. Freyer et al. (1993)
297 determined the annual average daytime $\delta(\text{NO}_2)$ - $\delta(\text{NO})$ at Julich, Germany along with average
298 daytime NO concentration (9 nmol mol^{-1} , similar to our experimental conditions) to be
299 $+18.03 \pm 0.98$ ‰. Using Eq. (7), assuming the daytime average $j(\text{NO}_2)$ value throughout the year
300 was $5.0 \pm 1.0 \times 10^{-3}$, and a calculated A value from measured NO_x concentration ranged from 0.22-
301 0.33, the average NO-NO₂ fractionation factor was calculated to be $+18.8 \pm 1.4$ ‰ (Fig. 1C), in
302 excellent agreement with the measurements in the present study. This agreement suggests the

303 NO+RO₂/HO₂ reactions might have similar fractionation factors as NO+O₃. Therefore, we suggest
304 Eq. (7) and (8) can be used to estimate the isotopic fractionations between NO and NO₂ in the
305 troposphere.

306

307 **3.3 Calculating nitrogen isotopic fractionations of NO-NO₂**

308 First, Eq. (7) was used to calculate the $\Delta(\text{NO}_2\text{-NO}) = \delta(\text{NO}_2) - \delta(\text{NO})$ at a wide range of
309 NO_x concentrations, $f(\text{NO}_2)$ and $j(\text{NO}_2)$ values (Fig. 2A-D). $j(\text{NO}_2)$ values of 0 s⁻¹ (Fig. 2A),
310 1.4×10^{-3} s⁻¹ (Fig. 2B), 5×10^{-3} s⁻¹ (Fig. 2C) and 1×10^{-2} s⁻¹ (Fig. 2D) were selected to represent
311 nighttime, dawn (as well as the laboratory conditions of our experiments), daytime average and
312 noon, respectively. Each panel represented a fixed $j(\text{NO}_2)$ value, and the $\Delta(\text{NO}_2\text{-NO})$ values were
313 calculated as a function of the A value, which was derived from NO_x concentration and $f(\text{NO}_2)$.
314 The A values have a large span, from 0 to 500, depending on the $j(\text{NO}_2)$ value and the NO
315 concentration. When A=0 ($j(\text{NO}_2)=0$) and $f(\text{NO}_2)<1$ (meaning NO-NO₂ coexist and [O₃]=0), Eq.
316 (7) and (8) become Eq. (2) and (3), showing the EIE was the sole factor, the $\Delta(\text{NO}_2\text{-NO})$ values
317 were solely controlled by EIE which has a constant value of +27.5 ‰ at 298K (Fig. 2A). When
318 $j(\text{NO}_2)>0$, the calculated $\Delta(\text{NO}_2\text{-NO})$ values showed a wide range from -10.0 ‰ (controlled by
319 LCIE factor: $\alpha_2 - \alpha_1 = -10$ ‰) to +27.5 ‰ (controlled by EIE factor: $\alpha(\text{NO}_2\text{-NO}) - 1 = +27.5$ ‰). Fig.
320 2B-D display the transition from a LCIE-dominated regime to an EIE-dominated regime. The
321 LCIE-dominated regime is characterized by low [NO_x] (<50 pmol mol⁻¹), representing remote
322 ocean areas and polar regions (Beine et al., 2002; Custard et al., 2015). At this range the A value
323 can be greater than 200, thus Eq. (7) can be simplified as: $\Delta(\text{NO}_2\text{-NO}) = (\alpha_2 - \alpha_1) \times 1000$ ‰,
324 suggesting the LCIE almost exclusively controls the NO-NO₂ isotopic fractionation. The $\Delta(\text{NO}_2\text{-}$
325 NO) values of these regions are predicted to be <0 ‰ during most time of the day and < -5 ‰ at

326 noon. On the other hand, the EIE-dominated regime was characterized by high $[\text{NO}_x]$ ($>20 \text{ nmol}$
327 mol^{-1}) and low $f(\text{NO}_2)$ (< 0.6), representative of regions with intensive NO emissions, e.g., near
328 roadside or stack plumes (Clapp & Jenkin, 2001; Kimbrough et al., 2017). In this case, the τ_{exchange}
329 are relatively short (10-50 s) compared to the τ_{photo} (approximately 100 s at noon and 1000 s at
330 dawn), therefore the A values are small (0.01-0.5). The EIE factor in this regime thus is much more
331 important than the LCIE factor, resulting in high $\Delta(\text{NO}_2\text{-NO})$ values ($>20 \text{ ‰}$). Between the two
332 regimes, both EIE and LCIE are competitive and therefore it is necessary to use Eq. (7) to quantify
333 the $\Delta(\text{NO}_2\text{-NO})$ values.

334 Fig. 2 also implies that changes in the $j(\text{NO}_2)$ value can cause the diurnal variations in
335 $\Delta(\text{NO}_2\text{-NO})$ values. Changing $j(\text{NO}_2)$ would affect the value of A and consequently the NO-NO₂
336 isotopic fractionations in two ways: 1) changes in $j(\text{NO}_2)$ value would change the photolysis
337 intensity, therefore the τ_{photo} value; 2) in addition, changes in $j(\text{NO}_2)$ value would also alter the
338 steady state NO concentration, therefore changing the τ_{exchange} (Fig. 2C). The combined effect of
339 these two factors on the A value varies along with the atmospheric conditions, and thus needs to
340 be carefully calculated using NO_x concentration data and atmospheric chemistry models.

341 We then calculated the differences of $\delta^{15}\text{N}$ values between NO₂ and total NO_x, e.g. $\Delta(\text{NO}_2\text{-}$
342 $\text{NO}_x) = \delta(\text{NO}_2) - \delta(\text{NO}_x)$ in Fig. 2E-H. Since $\Delta(\text{NO}_2\text{-NO}_x)$ are connected through the observed $\delta^{15}\text{N}$
343 of NO₂ (or nitrate) to the $\delta^{15}\text{N}$ of NO_x sources, this term might be useful in field studies (e.g.,
344 Chang et al., 2018; Zong et al., 2017). The calculated $\Delta(\text{NO}_2\text{-NO}_x)$ values (Fig. 2E-H) also showed
345 a LCIE-dominated regime at low $[\text{NO}_x]$ and an EIE-dominated regime at high $[\text{NO}_x]$. The $\Delta(\text{NO}_2\text{-}$
346 $\text{NO}_x)$ values were dampened by the $1-f(\text{NO}_2)$ factor comparing to $\Delta(\text{NO}_2\text{-NO})$, as shown in Eq.
347 (3) and (8): $\Delta(\text{NO}_2\text{-NO}_x) = \Delta(\text{NO}_2\text{-NO}) \times (1-f(\text{NO}_2))$. At high $f(\text{NO}_2)$ values (>0.8), the differences
348 between $\delta(\text{NO}_2)$ and $\delta(\text{NO}_x)$ were less than 5 ‰, thus the measured $\delta(\text{NO}_2)$ values were similar to

349 $\delta(\text{NO}_x)$, although the isotopic fractionation between NO and NO_2 could be noteworthy. Some
350 ambient environments with significant NO emissions or high NO_2 photolysis rates usually have
351 $f(\text{NO}_2)$ values between 0.4-0.8 (Mazzeo et al., 2005; Vicars et al., 2013). In this scenario, the
352 $\Delta(\text{NO}_2\text{-NO}_x)$ values in Fig. 2F-H showed wide ranges of -4.8 ‰ to +15.6 ‰, -6.0 ‰ to +15.0 ‰,
353 and -6.3 ‰ to +14.2 ‰ at $j(\text{NO}_2)=1.4\times 10^{-3} \text{ s}^{-1}$, $5\times 10^{-3} \text{ s}^{-1}$, $1\times 10^{-2} \text{ s}^{-1}$, respectively. These significant
354 differences again highlighted the importance of both LCIE and EIE (Eq. (7) and (8)) in calculating
355 the $\Delta(\text{NO}_2\text{-NO}_x)$. In the following discussion, we assume 1) the α_1 value remain constant (see
356 discussion above), 2) the $\text{NO}+\text{RO}_2/\text{HO}_2$ reactions have the same fractionation factors (α_2) as
357 $\text{NO}+\text{O}_3$, and 3) both EIE and LCIE do not display significant temperature dependence, then use
358 Equations (7) and (8) and this laboratory determined LCIE factor (-10 ‰) to calculate the nitrogen
359 isotopic fractionation between NO and NO_2 at various tropospheric atmospheric conditions.

360

361 **4. Implications**

362 The daily variations of $\Delta(\text{NO}_2\text{-NO}_x)$ values at two roadside NO_x monitoring sites were
363 predicted to demonstrate the effects of NO_x concentrations to the NO- NO_2 isotopic fractionations.
364 Hourly NO and NO_2 concentrations were acquired from a roadside site at Anaheim, CA
365 (<https://www.arb.ca.gov>) and an urban site at Evansville, IN (<http://idem.tx.sutron.com>) on July
366 25, 2018. The hourly $j(\text{NO}_2)$ values output from the TUV model (Madronich & Flocke, 1999) at
367 these locations was used to calculate the daily variations of $\Delta(\text{NO}_2\text{-NO}_x)$ values (Fig. 3A, B) by
368 applying Eq. (8). Hourly NO_x concentrations were 12-51 nmol mol^{-1} at Anaheim and 9-38 nmol
369 mol^{-1} at Evansville and the $f(\text{NO}_2)$ values at both sites did not show significant daily variations
370 (0.45 ± 0.07 at Anaheim and 0.65 ± 0.08 at Evansville), likely because the NO_x concentrations were
371 controlled by the high NO emissions from the road (Gao, 2007). The calculated $\Delta(\text{NO}_2\text{-NO}_x)$

372 values using Eq. (8) showed significant diurnal variations. During the nighttime, the isotopic
373 fractionations were solely controlled by the EIE, the predicted $\Delta(\text{NO}_2\text{-NO}_x)$ values were
374 $+14.5\pm 2.0$ ‰ and $+8.7\pm 2.1$ ‰ at Anaheim and Evansville, respectively. During the daytime, the
375 existence of LCIE lowered the predicted $\Delta(\text{NO}_2\text{-NO}_x)$ values to $+9.8\pm 1.7$ ‰ at Anaheim and
376 $+3.1\pm 1.5$ ‰ at Evansville while the $f(\text{NO}_2)$ values at both sites remained similar. The lowest
377 $\Delta(\text{NO}_2\text{-NO}_x)$ values for both sites ($+7.0$ ‰ and $+1.7$ ‰) occurred around noon when the NO_x
378 photolysis was the most intense. In contrast, if one neglects the LCIE factor in the daytime, the
379 $\Delta(\text{NO}_2\text{-NO}_x)$ values would be $+12.9\pm 1.5$ ‰ and $+10.0\pm 1.6$ ‰ respectively, an overestimation of
380 3.1 ‰ and 6.9 ‰. These discrepancies suggested that the LCIE played an important role in the
381 NO-NO_2 isotopic fractionations and neglecting it could bias the NO_x source apportionment using
382 $\delta^{15}\text{N}$ of NO_2 or nitrate.

383 The role of LCIE was more important in less polluted sites. The $\Delta(\text{NO}_2\text{-NO}_x)$ values
384 calculated for a suburban site near San Diego, CA, USA, again using the hourly NO_x
385 concentrations (<https://www.arb.ca.gov>, Fig. 3C) and $j(\text{NO}_2)$ values calculated from the TUV
386 model. NO_x concentrations at this site varied from 1 to 9 nmol mol^{-1} . During the nighttime, NO_x
387 was in the form of NO_2 ($f(\text{NO}_2) = 1$) because O_3 concentrations were higher than NO_x , thus the
388 $\delta(\text{NO}_2)$ values should be identical to $\delta(\text{NO}_x)$ ($\Delta(\text{NO}_2\text{-NO}_x) = 0$). In the daytime a certain amount
389 of NO was produced by direct NO emission and NO_2 photolysis but the $f(\text{NO}_2)$ was still high
390 (0.73 ± 0.08). Our calculation suggested the daytime $\Delta(\text{NO}_2\text{-NO}_x)$ values should be only $+1.3\pm 3.2$ ‰
391 with a lowest value of -1.3 ‰. These $\Delta(\text{NO}_2\text{-NO}_x)$ values were similar to the observed and modeled
392 summer daytime $\delta(\text{NO}_2)$ values in West Lafayette, IN (Walters et al., 2018), which suggest the
393 average daytime $\Delta(\text{NO}_2\text{-NO}_x)$ values at $\text{NO}_x = 3.9\pm 1.2$ nmol mol^{-1} should range from $+0.1$ ‰ to

394 +2.4 ‰. In this regime, we suggest the $\Delta(\text{NO}_2\text{-NO}_x)$ values were generally small due to the
395 significant contribution of LCIE and high $f(\text{NO}_2)$.

396 The LCIE should be the dominant factor controlling the NO-NO₂ isotopic fractionation at
397 remote regions, resulting in a completely different diurnal pattern of $\Delta(\text{NO}_2\text{-NO}_x)$ compared with
398 the urban-suburban area. Direct hourly measurements of NO_x at remote sites are rare, thus we used
399 total NO_x concentration of 50 pmol mol⁻¹, daily O₃ concentration of 20 nmol mol⁻¹ at Summit,
400 Greenland (Dibb et al., 2002; Hastings et al., 2004; Honrath et al., 1999; Yang et al., 2002), and
401 assumed the conversion of NO to NO₂ was completely controlled by O₃ to calculate the NO/NO₂
402 ratios. Here the isotopes of NO_x were almost exclusively controlled by the LCIE due to the high
403 A values (>110). The $\Delta(\text{NO}_2\text{-NO}_x)$ values displayed a clear diurnal pattern (Fig. 3D) with highest
404 value of -0.3 ‰ in the “nighttime” (solar zenith angle >85 degree) and lowest value of -5.0 ‰ in
405 the mid-day. This suggest that the isotopic fractionations between NO and NO₂ were almost
406 completely controlled by LCIE at remote regions, when NO_x concentrations were <0.1 nmol mol⁻¹.
407 ¹. However, since the isotopic fractionation factors of nitrate-formation reactions (NO₂+OH,
408 NO₃+HC, N₂O₅+H₂O) are still unknown, more studies are needed to fully explain the daily and
409 seasonal variations of $\delta(\text{NO}_3^-)$ at remote regions.

410 Nevertheless, our results have a few limitations. First, currently there are very few field
411 observations that can be used to evaluate our model, therefore, future field observations that
412 measure the $\delta^{15}\text{N}$ values of ambient NO and NO₂ should be carried out to test our model. Second,
413 more work, including theoretical and experimental studies, is needed to investigate the isotope
414 fractionation factors occurring during the conversion from NO_x to NO_y and nitrate: in the NO_y
415 cycle, EIE (isotopic exchange between NO₂, NO₃ and N₂O₅), KIE (formation of NO₃, N₂O₅ and
416 nitrate) and PHIFE (photolysis of NO₃, N₂O₅, HONO and sometimes nitrate) may also exist and

417 be relevant for the $\delta^{15}\text{N}$ of HNO_3 and HONO. In particular, the N isotope fractionation occurring
418 during the $\text{NO}_2 + \text{OH} \rightarrow \text{HNO}_3$ reaction needs investigation. Such studies could help us modeling
419 the isotopic fractionation between NO_x emission and nitrate, and eventually enable us to analyze
420 the $\delta^{15}\text{N}$ value of NO_x emission by measuring the $\delta^{15}\text{N}$ values of nitrate aerosols and nitrate in wet
421 depositions. Third, our discussion only focuses on the reactive nitrogen chemistry in the
422 troposphere, however, the nitrogen chemistry in the stratosphere is drastically different from the
423 tropospheric chemistry, thus future studies are also needed to investigate the isotopic fractionations
424 in the stratospheric nitrogen chemistry. Last, the temperature dependence of both EIE and LCIE
425 needs to be carefully investigated, because of the wide range of temperature in both troposphere
426 and stratosphere. Changes in temperature could alter the isotopic fractionation factors of both EIE
427 and LCIE, as well as contribute to the seasonality of isotopic fractionations between NO_x and NO_y
428 molecules.

429

430 **5. Conclusions**

431 The effect of NO_x photochemistry on the nitrogen isotopic fractionations between NO and
432 NO_2 was investigated. We first measured the isotopic fractionations between NO and NO_2 and
433 provided mathematical solutions to assess the impact of NO_x level and NO_2 photolysis rate ($j(\text{NO}_2)$)
434 to the relative importance of EIE and LCIE. The EIE and LCIE isotope fractionation factors, at
435 room temperature, were determined to be 1.0275 ± 0.0012 and 0.990 ± 0.005 , respectively. These
436 calculations and measurements can be used to determine the steady state $\Delta(\text{NO}_2\text{-NO})$ and $\Delta(\text{NO}_2\text{-}$
437 $\text{NO}_x)$ values at room temperature. Subsequently we applied our equations to polluted, clean and
438 remote sites to model the daily variations of $\Delta(\text{NO}_2\text{-NO}_x)$ values. We found that the $\Delta(\text{NO}_2\text{-NO}_x)$
439 values could vary from over +20 ‰ to less than -5 ‰ depending on the environment: in general,

440 the role of LCIE becoming more important at low NO_x concentrations, which tend to decrease the
441 $\Delta(\text{NO}_2\text{-NO}_x)$ values. Our work provided a mathematical approach to quantify the nitrogen isotopic
442 fractionations between NO and NO₂ that can be applied to many tropospheric environments, which
443 could help interpret the measured $\delta^{15}\text{N}$ values of NO₂ and nitrate in field observation studies.

444

445 **Acknowledgement**

446 We thank NCAR's Advanced Study Program granted to Jianghanyang Li. The National
447 Center for Atmospheric Research is operated by the University Corporation for Atmospheric
448 Research, under the sponsorship of the National Science Foundation. We also thank funding
449 support from Purdue Climate Change Research Center and A. H. Ismail Interdisciplinary Program
450 Doctoral Research Travel Award granted by Purdue University.

451 **Data Availability**

452 Data acquired from this study was deposited at Open Sciences Framework (Li, 2019,
453 DOI 10.17605/OSF.IO/JW8HU).

454 **Author contribution**

455 J. Li and G. Michalski designed the experiments, X. Zhang and J. Li conducted the
456 experiments. X. Zhang, G. Michalski, J. Orlando and G. Tyndall helped J. Li in interpreting the
457 results. The manuscript was written by J. Li and all the authors have contributed during the revision
458 of this manuscript.

459 **Competing interest**

460 The authors declare no competing interest.

461

462 **References:**

463

464 Atkinson, R., Baulch, D. L., Cox, R. A., Crowley, J. N., Hampson, R. F., Hynes, R. G., et al. (2004).
465 Evaluated kinetic and photochemical data for atmospheric chemistry: Volume I-gas phase
466 reactions of O_x, HO_x, NO_x and SO_x species. *Atmospheric Chemistry and Physics*, 4(6), 1461–1738.
467

468 Barney, W. S., & Finlayson-Pitts, B. J. (2000). Enhancement of N₂O₄ on porous glass at room
469 temperature: A key intermediate in the heterogeneous hydrolysis of NO₂? *The Journal of Physical
470 Chemistry A*, 104(2), 171–175.
471

472 Begun, G. M., & Fletcher, W. H. (1960). Partition function ratios for molecules containing
473 nitrogen isotopes. *The Journal of Chemical Physics*, 33(4), 1083–1085.
474

475 Begun, G. M., & Melton, C. E. (1956). Nitrogen isotopic fractionation between NO and NO₂ and
476 mass discrimination in mass analysis of NO₂. *The Journal of Chemical Physics*, 25(6), 1292–1293.
477

478 Beine, H. J., Honrath, R. E., Dominé, F., Simpson, W. R., & Fuentes, J. D. (2002). NO_x during
479 background and ozone depletion periods at Alert: Fluxes above the snow surface. *Journal of
480 Geophysical Research: Atmospheres*, 107(D21), ACH-7.
481

482 Bigeleisen, J., & Mayer, M. G. (1947). Calculation of equilibrium constants for isotopic exchange
483 reactions. *The Journal of Chemical Physics*, 15(5), 261–267.
484

485 Bigeleisen, J., & Wolfsberg, M. (1957). Theoretical and experimental aspects of isotope effects in
486 chemical kinetics. *Advances in Chemical Physics*, 15–76.
487

488 Casciotti, K. L., & McIlvin, M. R. (2007). Isotopic analyses of nitrate and nitrite from reference
489 mixtures and application to Eastern Tropical North Pacific waters. *Marine Chemistry*, 107(2), 184–
490 201.
491

492 Chang, Y., Zhang, Y., Tian, C., Zhang, S., Ma, X., Cao, F., et al. (2018). Nitrogen isotope
493 fractionation during gas-to-particle conversion of NO_x to NO₃⁻ in the atmosphere—implications for
494 isotope-based NO_x source apportionment. *Atmospheric Chemistry and Physics*, 18(16), 11647–
495 11661.
496

497 Clapp, L. J., & Jenkin, M. E. (2001). Analysis of the relationship between ambient levels of O₃,
498 NO₂ and NO as a function of NO_x in the UK. *Atmospheric Environment*, 35(36), 6391–6405.
499

500 Custard, K. D., Thompson, C. R., Pratt, K. A., Shepson, P. B., Liao, J., Huey, L. G., et al. (2015).
501 The NO_x dependence of bromine chemistry in the Arctic atmospheric boundary layer. *Atmospheric
502 Chemistry and Physics*, 15(18), 10799–10809.
503

504 Dibb, J. E., Arsenault, M., Peterson, M. C., & Honrath, R. E. (2002). Fast nitrogen oxide
505 photochemistry in Summit, Greenland snow. *Atmospheric Environment*, 36(15–16), 2501–2511.
506

507 Do Remus, R. H., Mehrotra, Y., Lanford, W. A., & Burman, C. (1983). Reaction of water with
508 glass: influence of a transformed surface layer. *Journal of Materials Science*, 18(2), 612–622.
509

510 Elliott, E. M., Kendall, C., Boyer, E. W., Burns, D. A., Lear, G. G., Golden, H. E., et al. (2009).
511 Dual nitrate isotopes in dry deposition: Utility for partitioning NO_x source contributions to
512 landscape nitrogen deposition. *Journal of Geophysical Research: Biogeosciences*, 114(G4),
513 G04020. <https://doi.org/10.1029/2008JG000889>
514

515 Felix, J. D., & Elliott, E. M. (2014). Isotopic composition of passively collected nitrogen dioxide
516 emissions: Vehicle, soil and livestock source signatures. *Atmospheric Environment*, 92, 359–366.
517

518 Felix, J. D., Elliott, E. M., & Shaw, S. L. (2012). Nitrogen isotopic composition of coal-fired power
519 plant NO_x: influence of emission controls and implications for global emission inventories.
520 *Environmental Science & Technology*, 46(6), 3528–3535.
521

522 Frey, M. M., Savarino, J., Morin, S., Erbland, J., & Martins, J. M. F. (2009). Photolysis imprint in
523 the nitrate stable isotope signal in snow and atmosphere of East Antarctica and implications for
524 reactive nitrogen cycling. *Atmos. Chem. Phys*, 9, 8681–8696.
525

526 Freyer, H. D. (1991). Seasonal variation of ¹⁵N/¹⁴N ratios in atmospheric nitrate species. *Tellus B*,
527 43(1), 30–44. <https://doi.org/10.1034/j.1600-0889.1991.00003.x>
528

529 Freyer, H. D., Kley, D., Volz-Thomas, A., & Kobel, K. (1993). On the interaction of isotopic
530 exchange processes with photochemical reactions in atmospheric oxides of nitrogen. *Journal of*
531 *Geophysical Research: Atmospheres*, 98(D8), 14791–14796.
532

533 Gao, H. O. (2007). Day of week effects on diurnal ozone/NO_x cycles and transportation emissions
534 in Southern California. *Transportation Research Part D: Transport and Environment*, 12(4), 292–
535 305.
536

537 Gobel, A. R., Altieri, K. E., Peters, A. J., Hastings, M. G., & Sigman, D. M. (2013). Insights into
538 anthropogenic nitrogen deposition to the North Atlantic investigated using the isotopic
539 composition of aerosol and rainwater nitrate. *Geophysical Research Letters*, 40(22), 5977–5982.
540 <https://doi.org/10.1002/2013GL058167>
541

542 Hastings, M G, Jarvis, J. C., & Steig, E. J. (2009). Anthropogenic impacts on nitrogen isotopes of
543 ice-core nitrate. *Science*, 324(5932), 1288.
544

545 Hastings, M G, Steig, E. J., & Sigman, D. M. (2004). Seasonal variations in N and O isotopes of
546 nitrate in snow at Summit, Greenland: Implications for the study of nitrate in snow and ice cores.
547 *Journal of Geophysical Research: Atmospheres*, 109(D20).
548

549 Hoefs, J. (2009). *Stable isotope geochemistry* (Vol. 285). Springer.
550

551 Honrath, R. E., Peterson, M. C., Guo, S., Dibb, J. E., Shepson, P. B., & Campbell, B. (1999).
552 Evidence of NO_x production within or upon ice particles in the Greenland snowpack. *Geophysical*
553 *Research Letters*, 26(6), 695–698.
554

555 Jarvis, J. C., Steig, E. J., Hastings, M. G., & Kunasek, S. A. (2008). Influence of local
556 photochemistry on isotopes of nitrate in Greenland snow. *Geophysical Research Letters*, 35(21).
557 Kendall, C., Elliott, E. M., & Wankel, S. D. (2007). Tracing anthropogenic inputs of nitrogen to
558 ecosystems. *Stable Isotopes in Ecology and Environmental Science*, 2, 375–449.
559
560 Kimbrough, S., Owen, R. C., Snyder, M., & Richmond-Bryant, J. (2017). NO to NO₂ conversion
561 rate analysis and implications for dispersion model chemistry methods using Las Vegas, Nevada
562 near-road field measurements. *Atmospheric Environment*, 165, 23–34.
563
564 King, Martin D., Carlos E. Canosa-Mas, and Richard P. Wayne. "Gas-phase reactions between
565 RO₂ and NO, HO₂ or CH₃O₂: correlations between rate constants and the SOMO energy of the
566 peroxy (RO₂) radical." *Atmospheric Environment* 35.12 (2001): 2081-2088.
567
568 Knote, Christoph, et al. "Influence of the choice of gas-phase mechanism on predictions of key
569 gaseous pollutants during the AQMEII phase-2 intercomparison." *Atmospheric Environment* 115
570 (2015): 553-568.
571
572 Li, J. (2019). Quantifying the nitrogen equilibrium and photochemistry-induced kinetic isotopic
573 effects between NO and NO₂. Retrieved from osf.io/jw8hu
574
575 Madronich, S., & Flocke, S. (1999). The role of solar radiation in atmospheric chemistry. In
576 *Environmental photochemistry* (pp. 1–26). Springer.
577
578 Mazzeo, N. A., Venegas, L. E., & Choren, H. (2005). Analysis of NO, NO₂, O₃ and NO_x
579 concentrations measured at a green area of Buenos Aires City during wintertime. *Atmospheric*
580 *Environment*, 39(17), 3055–3068.
581
582 McIlvin, M. R., & Altabet, M. A. (2005). Chemical conversion of nitrate and nitrite to nitrous
583 oxide for nitrogen and oxygen isotopic analysis in freshwater and seawater. *Analytical Chemistry*,
584 77(17), 5589–5595.
585
586 Michalski, G., Jost, R., Sugny, D., Joyeux, M., & Thiemens, M. (2004). Dissociation energies of
587 six NO₂ isotopologues by laser induced fluorescence spectroscopy and zero-point energy of some
588 triatomic molecules. *The Journal of Chemical Physics*, 121(15), 7153–7161.
589
590 Michalski, G., Bockheim, J. G., Kendall, C., & Thiemens, M. (2005). Isotopic composition of
591 Antarctic Dry Valley nitrate: Implications for NO_y sources and cycling in Antarctica. *Geophysical*
592 *Research Letters*, 32(13).
593
594 Miller, C. E., & Yung, Y. L. (2000). Photo-induced isotopic fractionation. *Journal of Geophysical*
595 *Research: Atmospheres*, 105(D23), 29039–29051.
596
597 Monse, E. U., Spindel, W., & Stern, M. J. (1969). Analysis of isotope-effect calculations illustrated
598 with exchange equilibria among oxynitrogen compounds. Rutgers-The State Univ., Newark, NJ.
599

600 Morin, S., Savarino, J., Frey, M. M., Domine, F., Jacobi, H.-W., Kaleschke, L., & Martins, J. M.
601 F. (2009). Comprehensive isotopic composition of atmospheric nitrate in the Atlantic Ocean
602 boundary layer from 65°S to 79°N. *J. Geophys. Res.*, 114. <https://doi.org/10.1029/2008JD010696>
603

604 Park, Y.-M., Park, K.-S., Kim, H., Yu, S.-M., Noh, S., Kim, M.-S., et al. (2018). Characterizing
605 isotopic compositions of TC-C, NO₃⁻-N, and NH₄⁺-N in PM_{2.5} in South Korea: Impact of China's
606 winter heating. <https://doi.org/10.1016/j.envpol.2017.10.072>
607

608 Saliba, N. A., Yang, H., & Finlayson-Pitts, B. J. (2001). Reaction of gaseous nitric oxide with
609 nitric acid on silica surfaces in the presence of water at room temperature. *The Journal of Physical*
610 *Chemistry A*, 105(45), 10339–10346.
611

612 Savarino, J., Morin, S., Erbland, J., Grannec, F., Patey, M. D., Vicars, W., et al. (2013). Isotopic
613 composition of atmospheric nitrate in a tropical marine boundary layer. *Proceedings of the*
614 *National Academy of Sciences*, 110(44), 17668–17673. <https://doi.org/10.1073/pnas.1216639110>
615

616 Sharma, H. D., Jervis, R. E., & Wong, K. Y. (1970). Isotopic exchange reactions in nitrogen oxides.
617 *The Journal of Physical Chemistry*, 74(4), 923–933.
618

619 Takei, T., Yamazaki, A., Watanabe, T., & Chikazawa, M. (1997). Water adsorption properties on
620 porous silica glass surface modified by trimethylsilyl groups. *Journal of Colloid and Interface*
621 *Science*, 188(2), 409–414.
622

623 Urey, H. C. (1947). The thermodynamic properties of isotopic substances. *Journal of the Chemical*
624 *Society (Resumed)*, 562-581.
625

626 Vicars, W. C., Morin, S., Savarino, J., Wagner, N. L., Erbland, J., Vince, E., et al. (2013). Spatial
627 and diurnal variability in reactive nitrogen oxide chemistry as reflected in the isotopic composition
628 of atmospheric nitrate: Results from the CalNex 2010 field study. *Journal of Geophysical Research:*
629 *Atmospheres*, 118(18), 10–567.
630

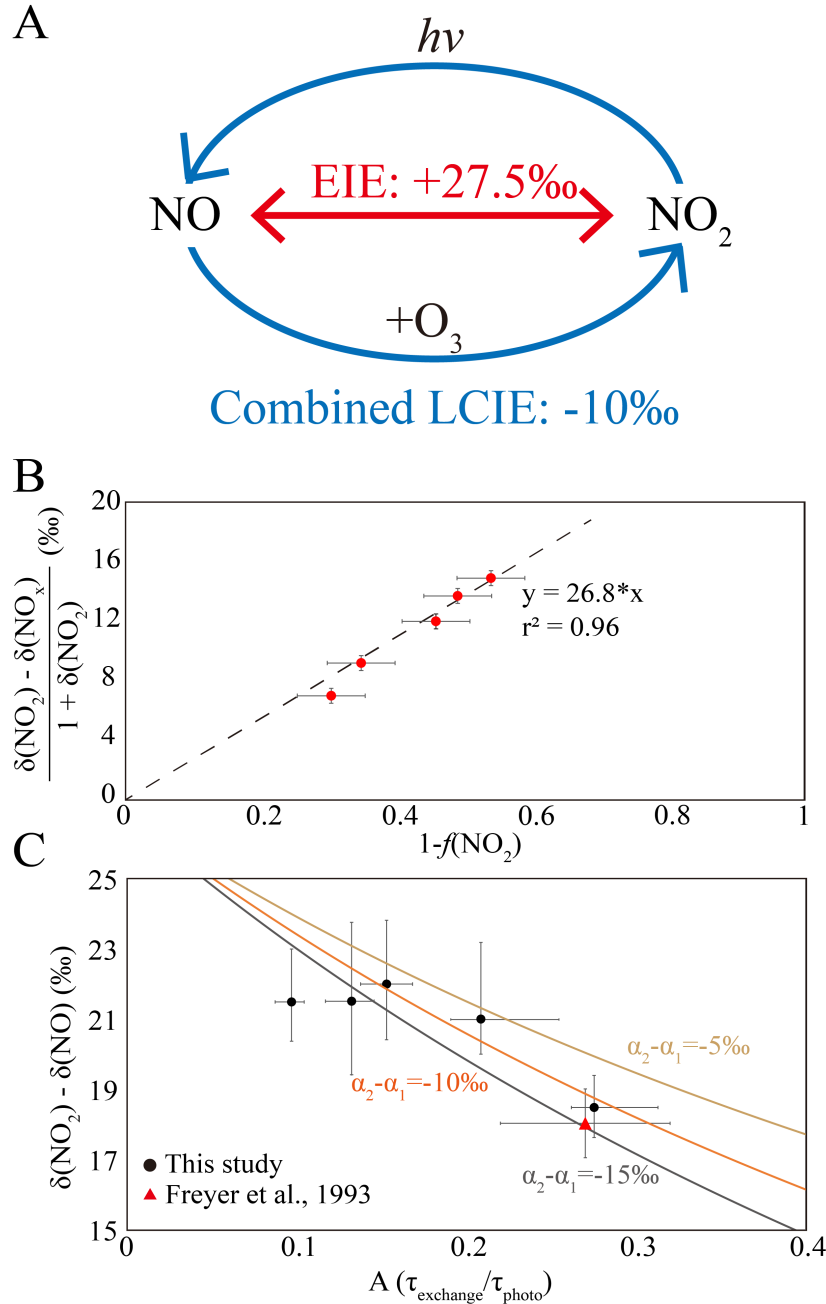
631 Walters, W. W., & Michalski, G. (2015). Theoretical calculation of nitrogen isotope equilibrium
632 exchange fractionation factors for various NO_y molecules. *Geochimica et Cosmochimica Acta*,
633 164, 284–297.
634

635 Walters, W. W., Goodwin, S. R., & Michalski, G. (2015). Nitrogen stable isotope composition
636 ($\delta^{15}\text{N}$) of vehicle-emitted NO_x. *Environmental Science & Technology*, 49(4), 2278–2285.
637

638 Walters, W. W., & Michalski, G. (2016). Ab initio study of nitrogen and position-specific oxygen
639 kinetic isotope effects in the NO+O₃ reaction. *The Journal of chemical physics*, 145(22), 224311.
640

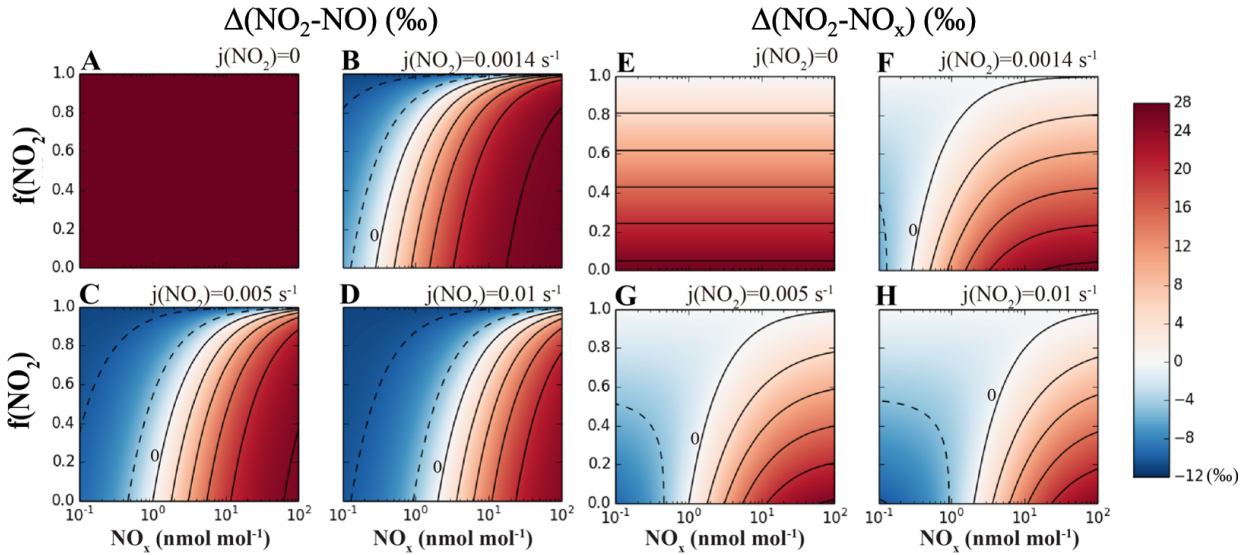
641 Walters, W. W., Simonini, D. S., & Michalski, G. (2016). Nitrogen isotope exchange between NO
642 and NO₂ and its implications for $\delta^{15}\text{N}$ variations in tropospheric NO_x and atmospheric nitrate.
643 *Geophysical Research Letters*, 43(1), 440–448.
644

- 645 Walters, W. W., Fang, H., & Michalski, G. (2018). Summertime diurnal variations in the isotopic
646 composition of atmospheric nitrogen dioxide at a small midwestern United States city.
647 *Atmospheric Environment*, 179, 1–11.
648
- 649 Williams, E. L., & Grosjean, D. (1990). Removal of atmospheric oxidants with annular denuders.
650 *Environmental Science & Technology*, 24(6), 811–814.
651
- 652 Yang, J., Honrath, R. E., Peterson, M. C., Dibb, J. E., Sumner, A. L., Shepson, P. B., et al. (2002).
653 Impacts of snowpack emissions on deduced levels of OH and peroxy radicals at Summit,
654 Greenland. *Atmospheric Environment*, 36(15–16), 2523–2534.
655
- 656 Zhang, X., Ortega, J., Huang, Y., Shertz, S., Tyndall, G. S., & Orlando, J. J. (2018). A steady-state
657 continuous flow chamber for the study of daytime and nighttime chemistry under atmospherically
658 relevant NO levels. *Atmospheric Measurement Techniques*, 11(5), 2537–2551.
659
- 660 Zong, Z., Wang, X., Tian, C., Chen, Y., Fang, Y., Zhang, F., et al. (2017). First assessment of NO_x
661 sources at a regional background site in North China using isotopic analysis linked with modeling.
662 *Environmental Science & Technology*, 51(11), 5923–5931.

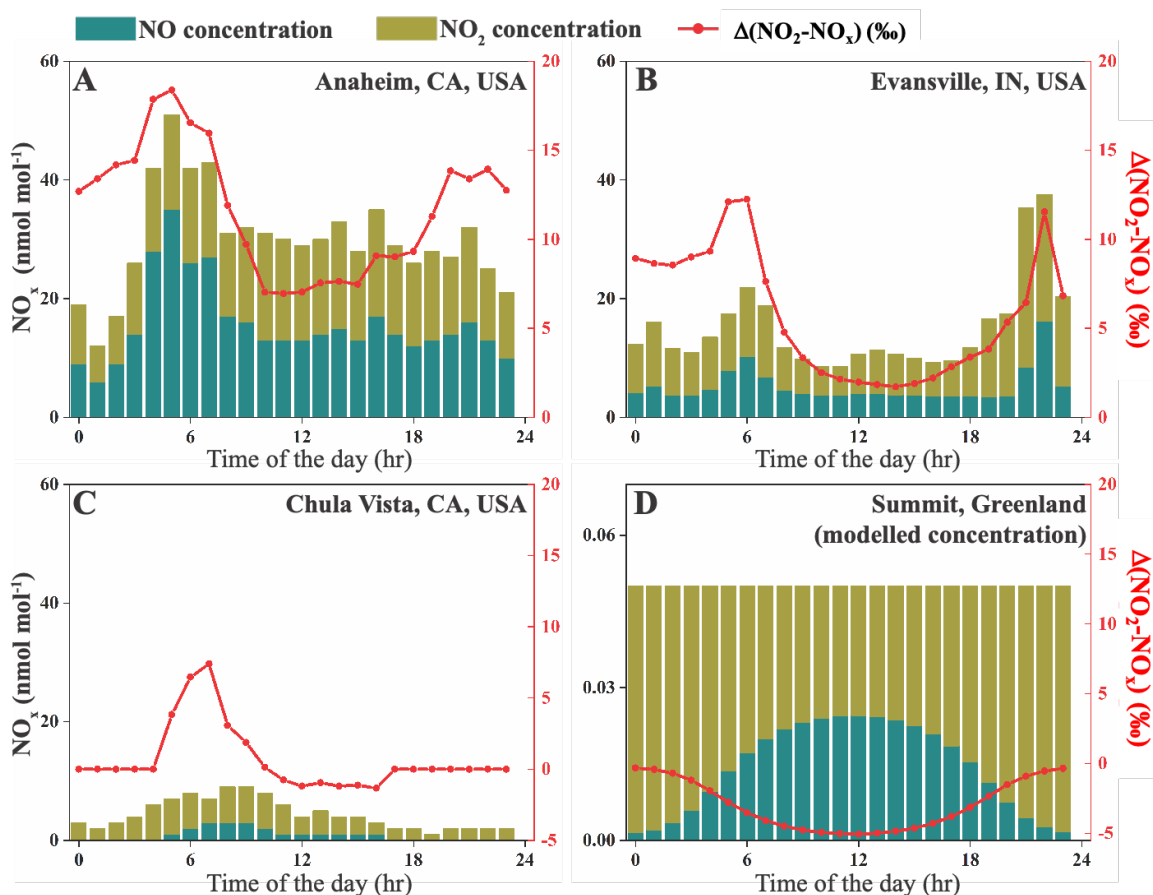


663
664
665
666
667
668
669
670
671

Fig. 1 **A.** a sketch of the isotopic fractionation processes between NO and NO₂, both fractionation factors are determined in this work. **B.** Results from five dark experiments yielded a line with $\epsilon(\text{NO}_2\text{-NO})/(1+\epsilon(\text{NO}_2\text{-NO}))$ value of 26.8 ‰ and $\epsilon(\text{NO}_2\text{-NO})$ value of 27.5 ‰; **C.** Results from five UV irradiation experiments (black points) and a previous field study (red triangle). The three lines represent different $(\alpha_2 - \alpha_1)$ values: the $(\alpha_2 - \alpha_1) = -10\text{‰}$ line showed the lowest RMSE to our experimental data as well as the previous field observation. The error bars in panels B and C represented the combined uncertainties of NO_x concentration measurements and isotopic analysis.



672
 673 **Fig. 2** Calculating isotopic fractionation values between NO-NO₂ ($\Delta(\text{NO}_2\text{-NO})$, **A-D**) and NO_x-
 674 NO₂ ($\Delta(\text{NO}_2\text{-NO}_x)$, **E-H**) at various $j(\text{NO}_2)$, NO_x level and $f(\text{NO}_2)$ using Eq. (7) and (8). Each
 675 panel represents a fixed $j(\text{NO}_2)$ value (showing on the upper right side of each panel), and the
 676 fractionation values are shown by color. Lines are contours with the same fractionation values, at
 677 an interval of 5‰, the contour line representing 0‰ was marked on each panel except for A and
 678 E.



679
 680 **Fig. 3** NO_x concentrations and calculated $\Delta(\text{NO}_2-\text{NO}_x)$ values at four sites. Stacked bars show the
 681 NO and NO₂ concentrations extracted from monitoring sites (A-C) or calculated using 0-D box
 682 model (D); the red lines are $\Delta(\text{NO}_2-\text{NO}_x)$ values at each site. Note that the NO_x concentration (left-
 683 y) axis on panel D is different from the rest.